Article ID: 1006-8775(2016) 04-0497-11

A CASE STUDY OF NUMERICAL SIMULATION OF SEA FOG ON THE SOUTHERN CHINA COAST

HUANG Hui-jun (黄辉军)[1], ZHAN Guo-wei (詹国伟)[2], LIU Chun-xia (刘春霞)[1], TU Jing (涂 静)[3], MAO Wei-kang (毛伟康)[1]

(1. Guangzhou Institute of Tropical and Marine Meteorology/Guangdong Provincial Key Laboratory of Regional Numerical Weather Prediction and Joint Open Laboratory of Marine Meteorology, CMA, Guangzhou 510080 China; 2. Maoming Meteorological Bureau, Maoming 525000 China; 3. Guangdong Meteorological Observatory, Guangzhou 510080 China)

Abstract: This study uses numerical simulations to examine a case of sea fog that was observed from 20 to 22 March 2011 on the southern China coast. The observation dataset includes observatory data, cloud-top temperature from MODIS, GPS sonde, and data from the Integrated Observation Platform for Marine Meteorology (IOPMM). The simulations are based on the Weather Research and Forecasting (WRF) model with four distinct parameter settings. Both the observations and simulations focus on the characteristics of the fog extent, boundary layer structure, and meteorological elements near the air-sea interface. Our main results are as follows: (1) The extent of mesoscale sea fog can be well simulated when the sea surface temperature has at least 0.5× 0.5 horizontal resolution. (2) To accurately model the vertical structure of the sea fog, particularly the surface-based inversion, vertical levels must be added in the boundary layer. (3) When these model conditions are met, the simulations faithfully reproduce the measured downward shortwave radiation, downward longwave radiation, and surface sensible heat flux during the sea fog period.

Key words: marine meteorology; sea fog; numerical simulation; southern China coast; scope; boundary layer characteristics

CLC number: P436.4 **Document code:** A

doi: 10.16555/j.1006-8775.2016.04.005

1 INTRODUCTION

Sea fog is a well-known hazard for marine navigation, harbor, and costal airport. These issues have spurred simulation studies on sea fog as well as the closely related marine stratocumulus and stratus. As early as the 1960s, Fisher and Caplan tried using a numerical method to forecast stratus and fog [1]. Other simulation studies of sea fog followed. However, despite the long history of numerical forecasting of sea fog, the topic still contains complex and difficult problems[2-3].

Lilly [4] simulated the cloud layer under a strong inversion, and discussed the effect of the entrainment. His simulation also demonstrated the importance of radiation cooling over fog top. Later, Barker[5] simulated sea fog on the west coast of America, using a two-dimensional boundary-layer model. The model took into account many factors, such as radiation transport, turbulence exchange and entrainment, cloud-droplet distribution, and the height of the boundary-layer. He pointed out that the radiative transfer processes are extremely important in the process of fog formation. He also found that humid air upstream favors fog occurrence. Soon afterwards, Oliver et al. [6] used a second-order closure model to analyze the turbulent and radiation effects. They also simulated advective-radiative fog, subsidence-capped stratus over the ocean, and surface fog resulting from the nocturnal of stratus. Focusing on the microphysics, Fitzgerald [7] investigated the formation and evolution of droplet spectra during the early formation stage of advection fogs at sea using a one-dimensional numerical model. The model was used to predict the evolution of the droplet-size distribution and visibility at an altitude of 20 m in two advection-type fogs off the coast of Nova Scotia in August 1975. The predicted droplet size distributions agreed well with impactor data. Ballard et al. [8] used the United Kingdom Meteorological Office (UKMO) mesoscale model to simulate the diurnal evolution of sea fog off the northeast Scottish coast observed on 27 April 1984. They pointed out that the accuracy of the early part of the forecast depends strongly on the specification of the initial conditions.

Received 2014-10-31; **Revised** 2016-10-10; **Accepted** 2016-11-15

Foundation item: National Natural Science Foundation of China (41275025; 41175013), Guangdong Science and Technology Plan Project (2008030303072, 2012A061400012), Meteorological Sciences Research Project (2013B06, 2013Q04, 2014B08), Early Warning and Forecasting Technology for Marine Meteorology of the Guangdong Meteorological Bureau

Biography: HUANG Hui-jun, Ph. D., Associate Professor, primarily undertaking research on air-sea boundary layer and marine meteorology

Corresponding author: HUANG Hui-jun, e-mail: hjhuang@grmc.gov.cn

Koračinet al.[9] simulated a case of fog formation along the California coast with a one-dimensional, higher-order, turbulence-closure model. They found that fog forms in response to relatively long preconditioning of the marine layer, and radiative cooling at the cloud top is the primary mechanism for cooling and mixing the cloud-topped marine layer. They also found that the processes of subsidence and cloud-top cooling are more important than the positive fluxes of sensible and latent heat at the air-sea interface. To examine further details, they later simulated the same case with a three-dimensional Mesoscale Model 5 (MM5) model[10].

Large-scale, dense sea fog often occurs in the Yellow Sea and East China Sea, motivating several modeling studies. For example, Hu and Zhou[11] analyzed the effects of air-sea conditions such as air temperature, humidity, wind, and sea-surface temperature (SST) on the process of sea fog using a two-dimensional model. Later, Fu et al.[12] simulated the liquid water content and other factors during the formation, development, and dissipation stages of a sea fog event on 1 June 1995. Then, they used the Regional Atmospheric Modeling System (RAMS) model to investigate a dense sea fog event that occurred over the Yellow sea on 11 April 2004 [13]. Gao et al.[14] used MM5 model to simulate a heavy sea-fog episode over the Yellow sea on 9 March 2005. The study used satellite images, surface observations, and soundings at islands and coasts to describe and analyze the event and found an extreme sensitivity to model input. In a follow-up, Gao et al.[15] processed the initial conditions of sea fog modeling over the Yellow sea using a cycling 3DVAR data assimilation scheme based on the Weather Research and Forecasting (WRF) model and its 3DVAR module. They found the initial-condition improvements crucial for modeling. More recently, Zhang and Ren[16] used the WRF model to simulate a sea fog event over the Yellow Sea on 2–3 May, 2008. They also investigated quantitatively the effect of the sea-surface thermal condition on the sea fog through sensitivity experiments, and the results show that the stability and turbulence under 100 m altitude are sensitive to the variations in the SST. Heo and Ha [17] examined the impact of air-sea coupling on advection fog and steam-fog events using a coupled atmosphere-ocean modeling system consisting of the Coupled Ocean-Atmosphere Mesoscale Prediction System (COAMPS) as the atmospheric component and the Regional Ocean Modeling System (ROMS) as the oceanic component. The coupled simulation showed that advection fog is controlled by low-level atmospheric stability and downward latent heat flux, with oceanic cooling through air-sea coupling. Kim and Yum [18] used a one-dimensional turbulence model, the PArameterized FOG (PAFOG) model, coupled with the WRF model to investigate the formation mechanism of a case of sea fog over the Yellow sea near the western coastal area of the Korean Peninsula. They found that the coupled model gave much better agreement with observations than did the WRF model alone. Li et al.[19] investigated a dense sea fog event that occurred over the Yellow Sea on 9 March 2005 using the WRF model with a newly implemented planetary boundary layer (PBL) scheme developed by Mellor-Yamada-Nakanishi-Niino (MYNN). The new scheme could reasonably reproduce the main features of this fog case. Zhao et al.[20] investigated the impact of SST on a heavy sea fog event over the Yellow Sea from 7–11 July 2008 using a mesoscale coupled air-sea model based on the WRF model and the regional Princeton Ocean Model (POM). The simulated pattern of fog calculated from the coupled model agreed well with the sea-fog region identified from the visible satellite imagery, better than that from the WRF model alone due to the more elaborate description of the SST in the coupled model.

Though the sea fog in the South China Sea is not as extensive as those in the Yellow Sea and East China Sea, it also results in severe catastrophes in this area. Here, the fog occurs from January to May, averaging 3–5 days per month from February to April, and appears about 100–200 km from the coast, usually surrounding the Leizhou Peninsula. The fog always forms in the afternoon or night, remaining through the next morning[21]. Since 2006, the Institute of Tropical and Marine Meteorology (ITMM) has made a series of observations of the boundary layer structure of the sea fog off the coast of southern China. Moreover, ITMM established the Marine Meteorological Science Experiment Base (MMSEB) at Bohe, Maoming since 2007. Lately, the Integrated Observation Platform for Marine Meteorology (IOPMM) set up in 2008 and acquired many observation datasets of sea fog. Based on these data, ITMM investigated the formation mechanism, the microphysics structure, and the characteristics of boundary layer of sea fog[22-27]. Regarding the forecast of the sea fog, ITMM developed a regional forecast based on the Global and Regional Assimilation Prediction System (GRAPES) together with the model output statistics (MOS) method[28-30]. Yuan and Huang[31] used the WRF model to simulate a case of sea fog near the mouth of the Pearl River on 21–22 March 2006. The results agreed well with the field observations. The purpose of this work is to improve our ability to simulate sea fog on the southern China coast, and also to provide a firm foundation for the numerical forecast of the sea fog in this area.

2 MODEL RUN AND CONTRASTIVE DATA

We run the Weather Research and Forecasting (WRF) model, version 3.5.1, with four distinct parameter settings (Table 1). The simulated period is from 0800 LST 20 to 0800 LST 23 March 2011. The four runs use the same atmospheric background field

Table 1. Settings for the simulation runs.

Name	Resolution of SST	Contrastive hour	Total vertical levels
run 1	FNL 1.0° × 1.0°	00 and 14 LST 21 March	Model generated 65 levels①
run 2	RTG 0.5° × 0.5°	00 and 14 LST 21 March	Model generated 65 levels
run 3	RTG 0.083° × 0.083°	14 LST 21 March	Model generated 65 levels
run 4	RTG 0.5° × 0.5°	00 LST 21 March	Manmade 66 levels②

from the National Centers for Environmental Prediction (NCEP) FNL (Final) Operational Global Analysis data (http://rda.ucar.edu/datasets/ds083.2).

For the time of 1400 LST 21 March, we compare runs 1, 2, and 3 to determine which setting best simulates the extent of the sea fog. The SST for run 1 comes from FNL data, with a 1.0° × 1.0° horizontal resolution, whereas the SST for runs 2 and 3 come from NCEP, with a 0.5° × 0.5° and 0.083° × 0.083° horizontal resolution, respectively.

For the time 0000 LST 21 March, we compare runs 1, 2, and 4 to determine which setting best simulates the vertical structure. The vertical levels of runs 1 and 2 are model generated with 65 levels, whereas those of run 4 are manmade with 66 levels. Within these 66 levels, 33 levels are under 2 000 m with an average vertical resolution of 63 m. The SST of run 4 is also the same as run 2 with 0.5° × 0.5° horizontal resolution. Additionally, the four runs are all compared with the surface observations made during the sea fog.

① σ levels: 1.0000, 0.9930, 0.9830, 0.9700, 0.9540, 0.9340, 0.9090, 0.8800, 0.8614, 0.8427, 0.8241, 0.8055, 0.7701, 0.7360, 0.7030, 0.6711, 0.6403, 0.6107, 0.5820, 0.5544, 0.5277, 0.5020, 0.4773, 0.4534, 0.4304, 0.4082, 0.3869, 0.3663, 0.3466, 0.3275, 0.3092, 0.2916, 0.2747, 0.2585, 0.2428, 0.2278, 0.2134, 0.1996, 0.1863, 0.1736, 0.1614, 0.1497, 0.1385, 0.1278, 0.1176, 0.1079, 0.0987, 0.0901, 0.0819, 0.0743, 0.0670, 0.0602, 0.0538, 0.0477, 0.0420, 0.0366, 0.0315, 0.0267, 0.0222, 0.0179, 0.0139, 0.0101, 0.0066, 0.0032, 0.0000

② σ levels: 1.0000, 0.9980, 0.9950, 0.9910, 0.9860, 0.9820, 0.9780, 0.9740, 0.9700, 0.9660, 0.9620, 0.9580, 0.9540, 0.9500, 0.9460, 0.9420, 0.9380, 0.9320, 0.9260, 0.9200, 0.9140, 0.9080, 0.9000, 0.8900, 0.8800, 0.8700, 0.8600, 0.8500, 0.8400, 0.8300, 0.8200, 0.8100, 0.8000, 0.7850, 0.7620, 0.7315, 0.7084, 0.6573, 0.6090, 0.5634, 0.5204, 0.4798, 0.4415, 0.4055, 0.3716, 0.3397, 0.3097, 0.2815, 0.2551, 0.2303, 0.2071, 0.1854, 0.1651, 0.1461, 0.1284, 0.1118, 0.0965, 0.0822, 0.0689, 0.0566, 0.0452, 0.0346, 0.0249, 0.0159, 0.0076, 0.0000.

All four runs use two-nested grids with the center grid point at 112.237° E, 21.385° N. The outer grid has 93 × 90 horizontal grid points with a 27-km horizontal resolution, whereas the inner grid has 166 × 157 horizontal grid points with a 9-km horizontal resolution. The WRF model use a 60-s time step, a 50-hPa model top level, and either a model-generated 65 vertical levels or a manmade 66 vertical levels. The main physical parameter schemes are as follows: RRTM[32] for the longwave radiation, Duhia [33] for the shortwave radiation, Noah [34] for the land surface, M-O similarity[35] for the surface layer, YSU [36] for the planetary boundary layer, Lin [37] for the microphysics, and finally New Kain-Fritsch [38] for the cumulus parameterization, but only in the outer grid.

Most of the observation data comes from the MMSEB (21.45° N, 111.32° E, 7.0 m MSL) and the IOPMM(21.44°N, 111.39°E)[39]. The MMSEB is only 50 m from the sea, whereas the IOPMM lies just offshore over water about 15 m deep, about 8.2 km eastward from MMSEB, and about 6.5 km from the nearest coast (Fig.1).

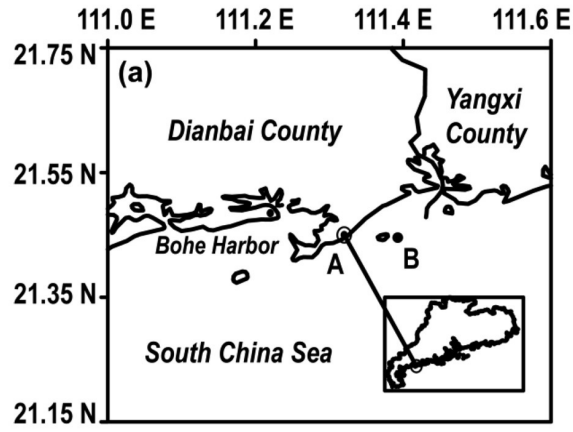

Figure 1. Observational site locations. Site A is MMSEB and site B is IOPMM.

GPS sondes (Vaisala model RS-92) were released from the IOPMM, and the sonde measurement accuracies are 0.2 K for temperature, 2% for humidity, 0.5 hPa for pressure, 2° for wind direction, and 0.15 m s^{-1} for wind speed. A sonde was released every 2 h on the even hours, namely 0000, 0200, 0400, 0600, and 0800 LST 21 March. The sampling rate is 0.5 Hz and the vertical resolution is 4-10 m. To achieve uniform data, the GPS sonde data are interpolated in the vertical with a 10-m interval. Calculation of the equivalent potential temperature (θ_e) follows Bolton (1980) [40]. Radiation, heat fluxes, and vertical velocity data come from the IOPMM. In particular, the radiation instrument (CNR_4 from Kipp&Zonen) is about 12 m above sea level, whereas the heat fluxes and vertical velocity

instrument (R3 –50 from Gill and LI7500A from LI-COR) are about 27.3 m above sea level. For more information about these instruments see Huang et al.[27].

Atmospheric visibility data was collected from the Meteorological Information Comprehensive Analysis and Process System (MICAPS)[41]. We use eddypro 4.0 software (http: // www.licor.com/env/products/eddy_covariance/software.html) to calculate turbulence flux over time intervals of 30 min. The software uses the Foken et al. method[42] to run quality control runs of the fluxes. We use cloud-top temperature data from MODIS (the Level 1 and Atmosphere Archive and Distribution System, LAADS) website[43]. We calculate the backward airflow trajectories by using the HYSPLIT trajectory model and the reanalysis data from the Global Data Assimilation System (GDAS)[44]. The SST data come from the Real Time Global data (RTG High Res 0.083, http://polar.ncep.noaa.gov/sst/) from the National Centers for Environmental Prediction (NCEP)[45].

3 THE PROCESS OF SEA FOG

The sea fog event here is an example of warm-advection sea fog in which the surface air temperature (SAT) exceeds the SST [27], followed by a cold front. In this event, the daytime of 20 March 2011 had a uniformly overcast sky with stratocumulus opacus and a light fog over the sea giving a visibility of about 5 km. According to the cloud-top temperature data from MODIS, on 1315 LST 20 March, the fog had already occurred over sea, and expanded toward the coast (Fig. 2a). From the large-scale synoptic background, wind transport had been continuously bringing warm, moist air from the warm sea surface to the 6-℃ colder sea surface near the coast. This situation led to sea fog (Fig.3a).

Relative humidity (RH) data of the IOPMM indicates sea fog appearing on 2240 LST 20 March, and lasting until 0050 LST 22 March (Fig.4a). Here, following previous observations, RH>=98% is consider as fog. According to the atmospheric visibility data of station observations, most of the southern China coast had sea fog on 0500 LST 21 March (Fig.3b). According to MODIS data, on 1415 LST 21 March (Fig.2b) the sea fog crossed the coastal line and extended inland. During the sea fog, the temperature increased, with the SAT exceeding the SST by an average of 1.9 ℃ (Fig. 4a). The surface wind direction is easterly to southeasterly before the sea fog, but transforms gradually from easterly to northeasterly during the sea fog period. Meanwhile, the wind speed remains between 4 and 6 m/s (Fig.4b). The sea fog layer is thick, so the short-wave radiation is no more than 692 W/m^2 (Fig.4c). Downward long-wave radiation is higher than upward long-wave radiation by 6.8 W/m^2 on average because the SAT always exceeds the SST during the sea fog period (Fig.4d).

While the cold front approaches via a continuous northeasterly wind, the RH decreases and the sea fog dissipates (Fig.4a –b). Observations showed that stratocumulus translucidus mostly covered the sky at the MMSEB after 1100 LST 22 March. By this time, the atmospheric visibility has increased to about 30 km.

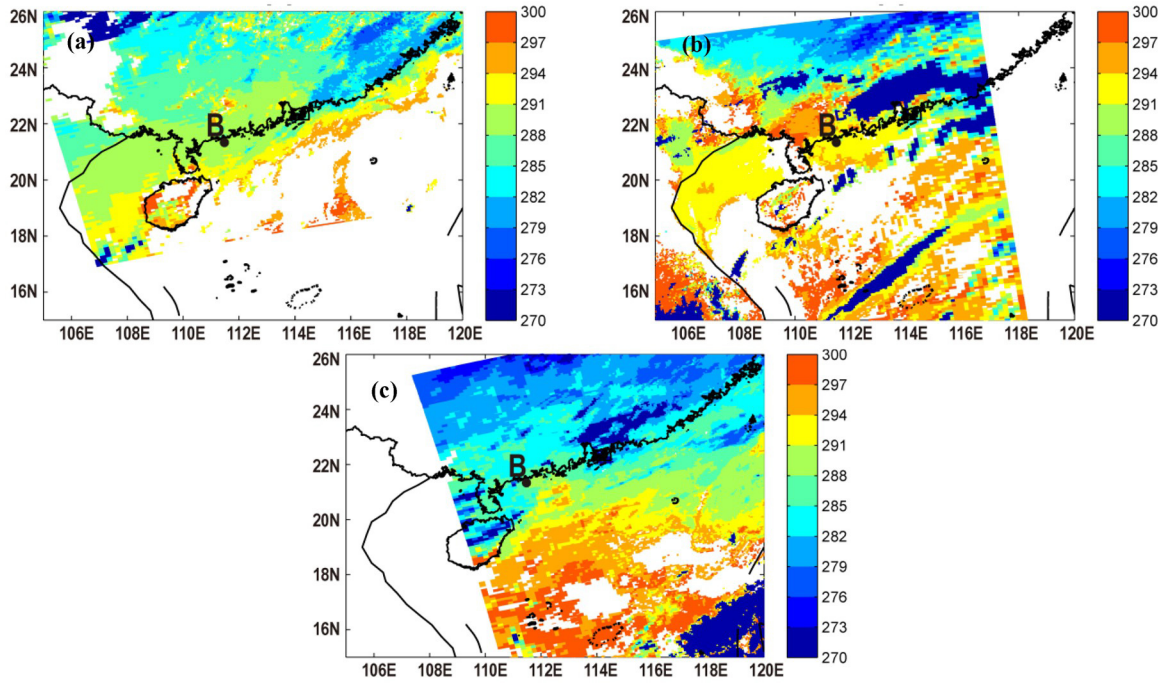

Figure 2. Cloud-top temperature (K) of the sea-fog events. The yellow represents the fog-top temperature, which is 291–294 K here. (a) 1335 LST 20 March, before the warm-advection fog. (b) 1415 LST 21 March, during the warm-advection fog. (c) 1320 LST 22 March, after the warm-advection fog. (From MODIS: http://ladsweb.nascom.nasa.gov/data/search.html.)

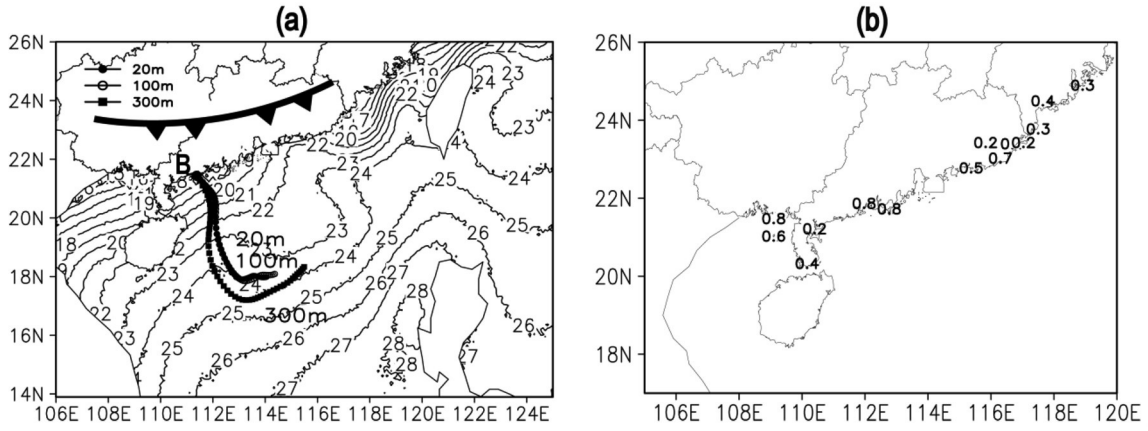

Figure 3. Synoptic background and the observed visibility.

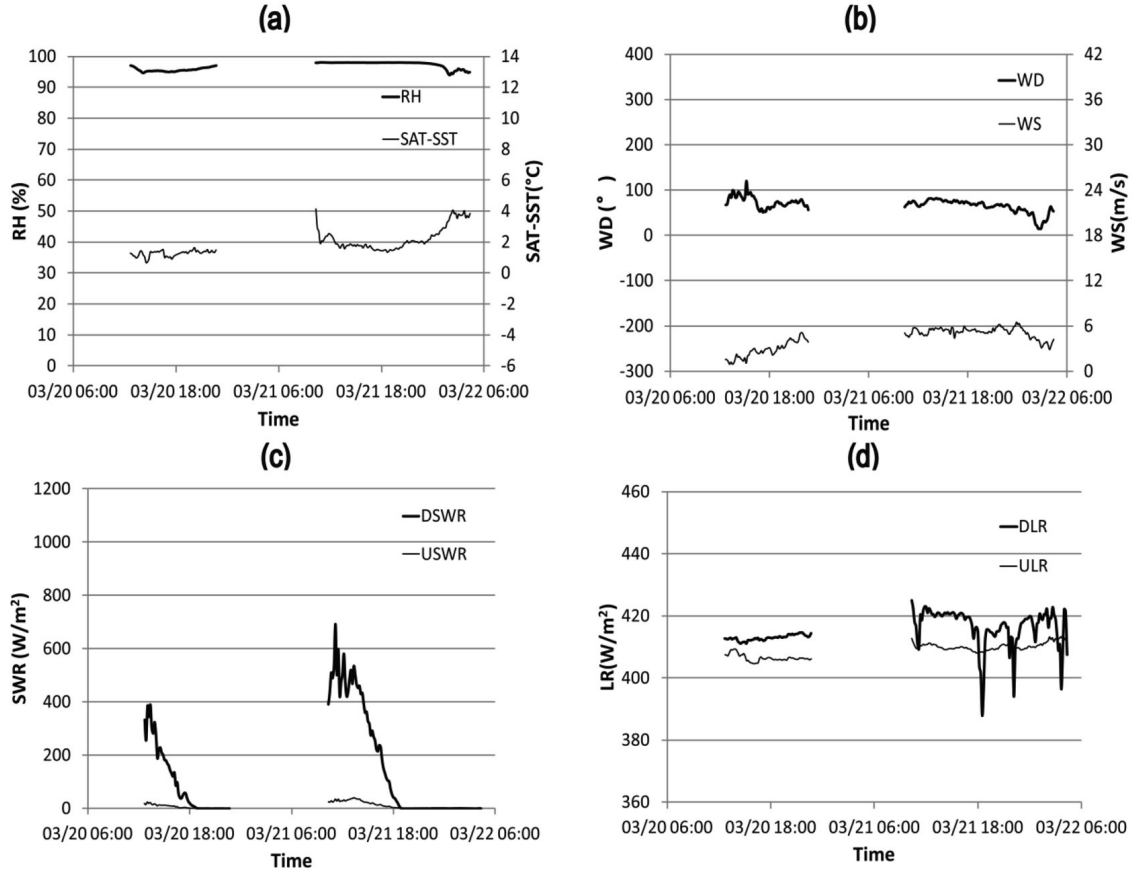

Figure 4. Meteorological parameters of the warm-advection fog case observed on the IOPMM. (a) RH = relative humidity. SAT-SST = difference of air and sea temperature. (b) Wd = wind direction, Ws = wind speed. (c) DSWR = downward short wave radiation, USWR = upward short-wave radiation. (d) DLR = downward long-wave radiation, ULR = upward long-wave radiation.

MODIS data shows that the cold front pushes the sea fog offshore on 1320 LST 22 March (Fig.2c).

4 SIMULATED RESULTS COMPARED WITH OBSERVATIONS

4.1 *Extent of the sea fog: dependence on SST horizontal resolution*

We ran three runs. For run 1, the horizontal resolution in SST was 1.0° × 1.0°; for run 2, 0.5° × 0.5°; and for run3, 0.083° × 0.083°. The results show that as the resolution becomes finer, the SST near the coastal area decreases (Fig.5).

Consider the liquid water content (LWC) pattern of three runs. We define the boundary of the sea fog as the region with LWC = 0.01 g/m^3, which is equivalent to an atmospheric visibility of 1.0 km [24]. The resulting fog

extent in run 1 is the worse one due to an error in the simulation offshore of the western part of Guangdong coast (Fig.2b, Fig.6a). Fig.6 shows that the simulated extent of sea fog in runs 2 and 3 are better than that of run 1. But runs 2 and 3 are each better at simulating different regions: offshore of the western part of Guangdong coast is better simulated by run 2, whereas the offshore region southwest of Hainan Island is better treated by run 3 (Fig.2b, Fig.6b-c). Thus, in general, an increase of the SST horizontal resolution can improve the simulated scope of the large-scale sea fog, but the improvement is not continuous. The result is quite good with 0.5° × 0.5° horizontal SST resolution.

4.2 *Vertical structure of sea fog: dependence on vertical levels*

The GPS sonde observations show that the low-level, warm, moist advection has a height of the surface-based inversion is about 200 m, and this height has the highest temperature in the boundary layer. However, the simulated inversion heights from runs 1 and 2 instead show a height of about 600 m. In run 4, the result is much better, with a simulated inversion at about 200 m (but this is not the highest temperature in the boundary layer), which demonstrates that an increase in the vertical levels in boundary layer helps to better simulate the surface-based inversion (Fig.7).

The simulated formation and dissipation time of sea fog of these three runs (1, 2, and 4) agree well with observations. For example, before and after 0400 LST 21 March, the simulation of RH near fog top shows a transition of high RH to lower RH in good agreement with observations (Fig.8a-d). However, the simulated fog top in the three runs are about 400 m, which is lower than the observed fog top of about 600-700 m (Fig.8a-d).

We now compare the simulated and observed profiles in the boundary layer on 0000 LST 21 March. According to the temperature profile in Fig.9, only run 4 accurately simulated the surface-based inversion. Compared to run 1, runs 2 and 4 more accurately depict the decrease in value closes to the sea surface. This behavior is due to the finer SST horizontal resolution of these two runs, which more accurately depict the low value area of SST along the coast. This phenomenon also occurred in the mixing ratio profile.

Consider now the wind profiles. For the wind direction profile, all three runs successfully simulated the warm advection, but they show more variation in direction than that of the observations. For example, the simulations show the wind direction transforming from easterly at the sea surface to southerly at the upper levels within 200 m, in contrast to the observed 400 m. Of all profiles, wind speed is the most difficult for the simulations. In particular, the observed wind speed increases gradually from the surface, reaching a maximum value at about 1 000 m. However, the simulated wind speed instead has a maximum value at about 500 m, with a decrease between 500 to 1 200 m.

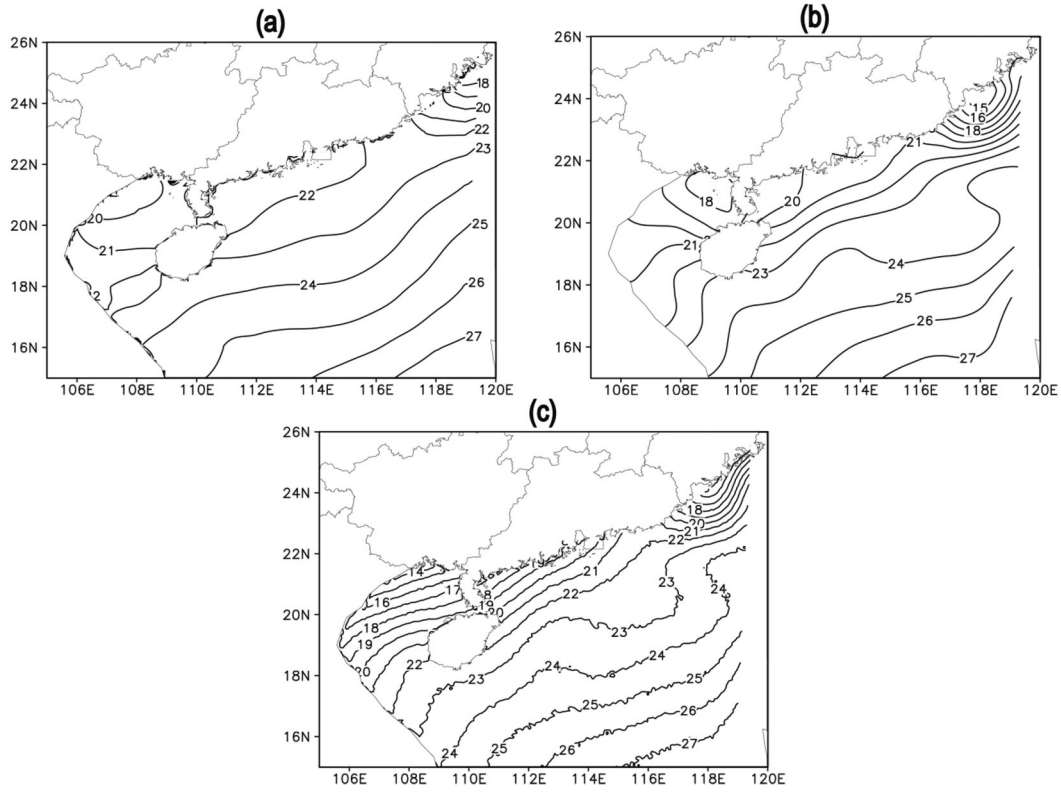

Figure 5. SST from three model runs with initial time of 0800 LST 20 March. Run 1, 1.0°×1.0°. (b) Run 2, 0.5°×0.5°. (c) Run 3, 0.083°×0.083°.

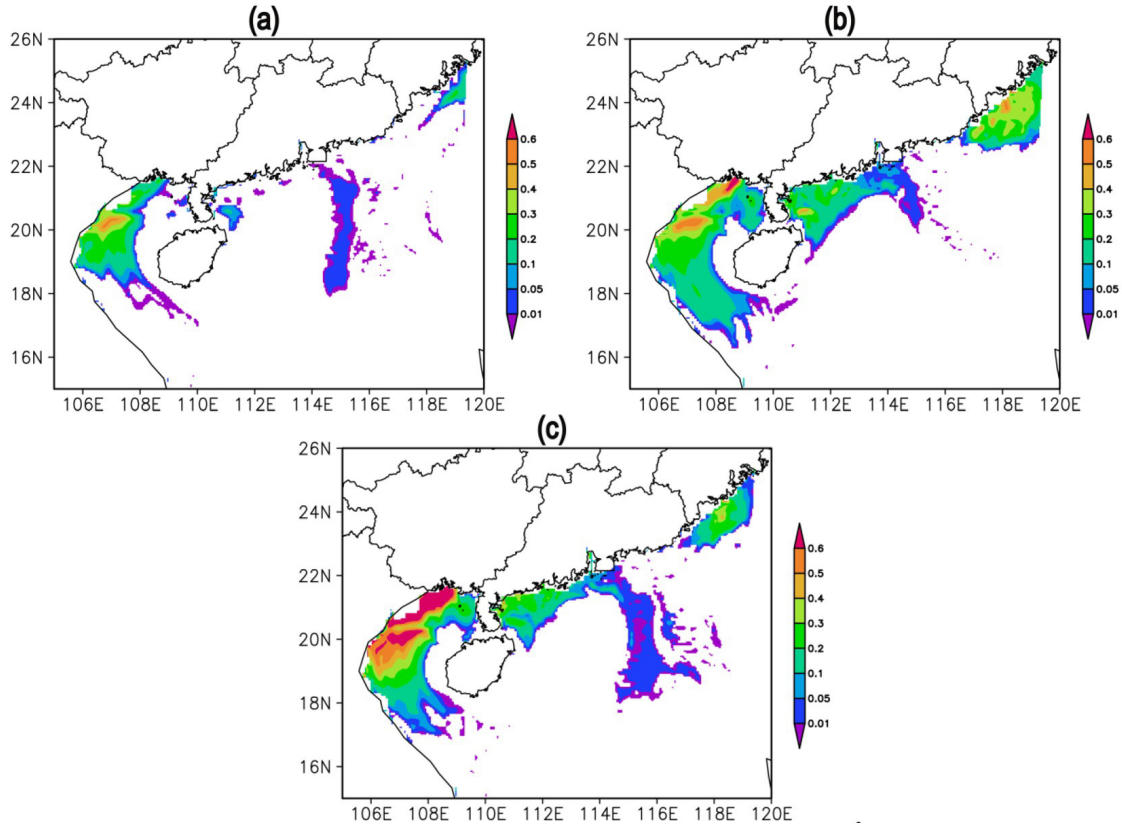

Figure 6. Liquid water content (LWC) distribution at 40 m on 1400LST 21 March (g/m^3). Run 1. (b) Run 2. (c) Run 3.

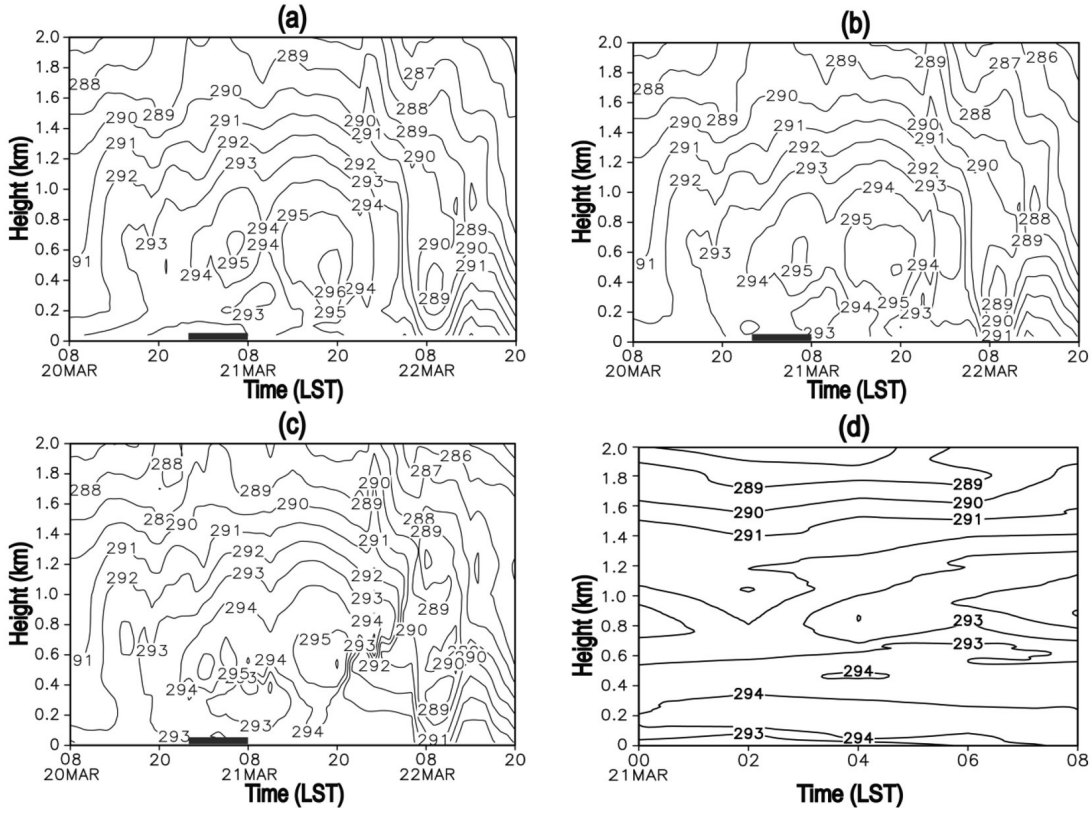

Figure 7. Temperature evolution of the atmospheric boundary layer: simulations and observations. (a) Simulated 60-h evolution of temperature of the atmospheric boundary layer from run 1. The shaded bar on the abscissa marks the time period of the observations in (d). (b) Same as (a) except for run 2, (c) Same as (a) except for run 4. (d) Observed temperature from the GPS sonde during 0000-0800 LST 21 March.

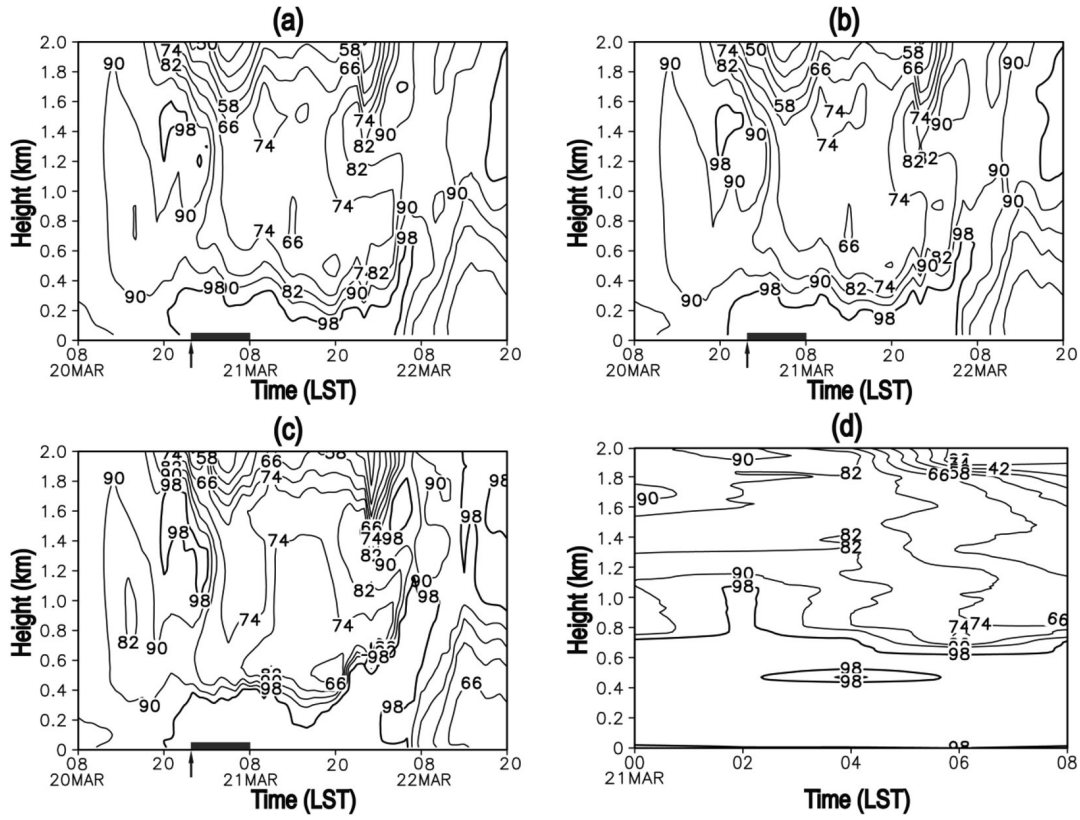

Figure 8. The same as Fig.7, but for relative humidity. The arrow on the abscissa is the time for the profile analysis in Fig. 9.

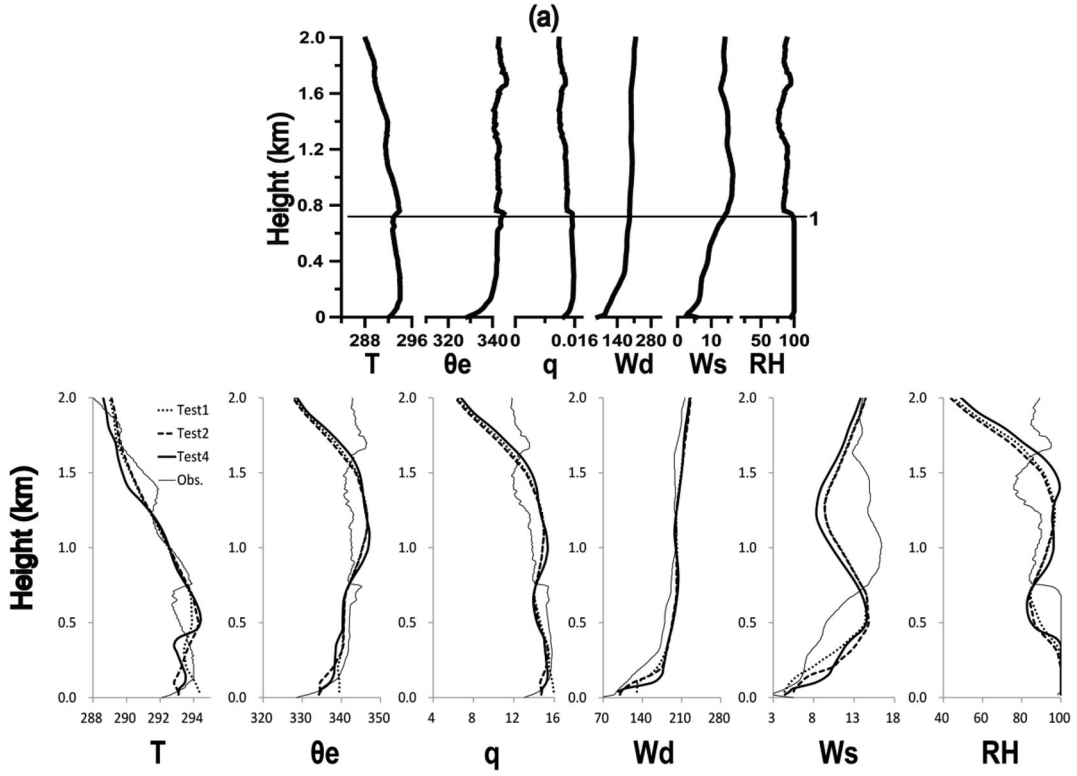

Figure 9. Comparison of profiles of meteorological parameters between three runs and GPS sonde observation on 0000 LST 21 March.

Thus, the simulated wind speed has a wind shear between 500 and 1 200 m and an increase of mechanical turbulence, which will eventually cause the sea fog to dissipate [46]. This model-produced dissipation process may be the cause of the decrease in simulated fog-top height.

4.3 *Simulated and observed parameters at the air−sea interface*

Consider now the parameters at the air-sea interface. First, the radiation. The simulated downward short-wave radiation is too high during the daytime of 20 March, indicating that the model cannot accurately simulate low clouds and light fog. But, compared to run 1, the other three simulations give good results in the heavier daytime fog on 21 March (Fig.10a). Because the model has difficulty with low clouds and light fog, the downward long-wave radiation is poorly simulated before the fog forms, but gives better results during the sea fog period (Fig 10b).

Concerning the surface heat fluxes, runs 2, 3, and 4 correctly simulate the sign and approximate magnitude of the sensible heat flux (Fig.10c). However, the values of the simulated vertical velocity are not even the same order as the observed values, and do not reveal the downward vertical velocity during the sea-fog period (Fig.10d). Finally, in the simulations, the latent heat flux is always zero, whereas the observations [27] give an average value of −6.22 W/m^2. The discrepancy is likely a consequence of the limited physical parameter scheme of the model.

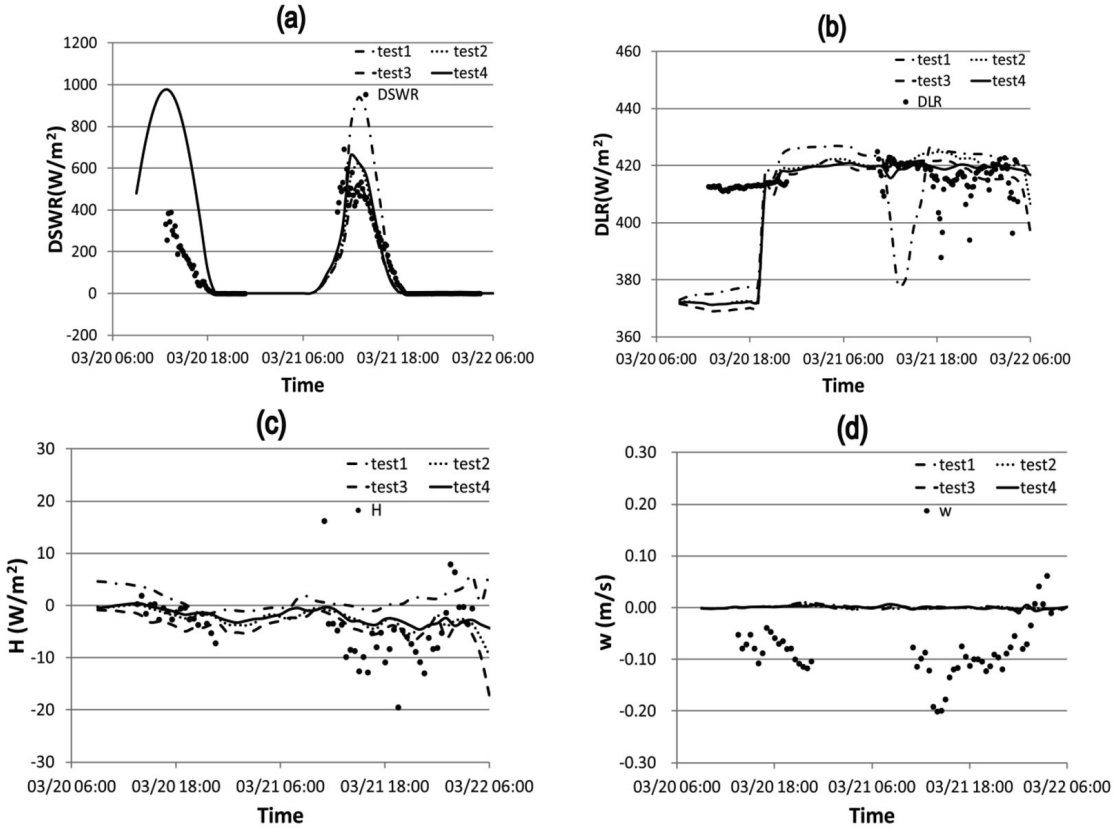

Figure 10. Comparison of air-sea meteorological parameters between four runs and IOPMM observation.

5 CONCLUSION AND DISCUSSION

We used the WRF model to simulate an observed warm-advection sea fog case on the Southern China coast. Our main conclusions are as follows:

(1) Using a 0.5°×0.5° SST horizontal resolution, the simulated mesoscale sea-fog pattern agreed well with observations.

(2) An increase of the vertical levels improved the simulated vertical structure; for example, giving a better simulation of the surface-based inversion.

(3) The model well simulated the downward shortwave radiation, the downward longwave radiation, and the sensible heat flux from the sea surface.

An accurate initial meteorological model field is essential for an accurate simulation of the sea fog on the south China coast, particularly because the extent of the sea fog here is smaller than those in the Yellow Sea and East China Sea. Concerning the SST, we found in the simulations that an increase of the SST will increase the temperature and the potential equivalent temperature close to the sea surface, which will lead to a failure of

the surface-based inversion and sea fog. Concerning the vertical profiles, we found that a poorly simulated maximum temperature in the boundary-layer profile affected the vertical structure of the sea fog. Moreover, a poorly simulated wind profile will produce false mechanical turbulence, which gives rise to a lower simulated fog top. Finally, concerning the initial conditions, a poorly initialized meteorological model field also resulted in no simulated low cloud and a light fog that existed before the sea fog. Additionally, the results indicate that the WRF model needs to improve. For example, the simulated vertical velocity is too small, and the latent heat flux is always zero. We aim to remedy these model deficiencies in future studies.

Acknowledgement: We thank supervisor and colleagues in Desert Research Institute (DRI), namely Darko Koračin, John Lewis, John Mejia, Eric Wilcox and Travis McCord, for their kindly suggestions and comments greatly improve this work. Special thanks to the crew of the Marine Meteorological Science Experiment Base at Bohe, for their help in conducting the field program and providing the data.

REFERENCES:

[1] FISHER E L, CAPLAN P. An experiment in numerical prediction of fog and stratus [J]. J Atmos Sci, 1963, 20 (5): 425-437.

[2] LEWIS J M, KORAČIN D, REDMOND K T. Sea fog research in the United Kingdom and United States - A historical essay including outlook [J]. Bull Amer Meteorol Soc, 2004, 85 (3): 395-408.

[3] KORAČIN D, Dorman C E, LEWIS J M, et al. Marine fog: A review [J]. Atmos Res, 2014, 143: 142-175.

[4] LILLY D K. Models of cloud-topped mixed layers under a strong inversion [J]. Quart J Roy Meteorol Soc, 1968, 94 (401): 292-309.

[5] BARKER E H. A maritime boundary-layer model for the prediction of fog [J]. Bound -Layer Meteor, 1977, 11 (3): 267-294.

[6] OLIVER D A, LEWELLEN W S, WILLIAMSON G G. The Interaction between Turbulent and Radiative Transport in the Development of Fog and Low-Level Stratus [J]. J Atmos Sci, 1978, 35 (2): 301-316.

[7] FITZGERALD J W. A Numerical Model of the Formation of Droplet Spectra in Advection Fogs at Sea and Its Applicability to Fogs off Nova Scotia [J]. J Atmos Sci, 1978, 35 (8): 1 522-1 535.

[8] BALLARD S P, GOLDING B W, SMITH R N B. Mesoscale model experimental forecasts of the HAAR of northeast Scotland [J]. Mon Wea Rev, 1991, 119 (9): 2 107-2 123.

[9] KORAČIN D, LEWIS J, THOMPSON W T, et al. Transition of stratus into fog along the California coast: Observations and modeling [J]. J Atmos Sci, 2001, 58 (13): 1 714-1 731.

[10] KORAČIN D, BUSINGER J, DORMAN C, et al. Formation, evolution, and dissipation of coastal sea fog [J]. Bound-Layer Meteor, 2005, 117 (3): 447-478.

[11] HU R J, ZHOU F X. A numerical study on the effects of air-sea conditions on the process of sea fog [J]. Period Ocean Univ China, 1997, 27(3): 282-290 (in Chinese).

[12] FU G, ZHANG T, ZHOU F X. Three-dimensional numerical simulation of real sea fog event over the Yellow Sea [J]. Period Ocean Univ China, 2002, 32(06): 859-867 (in Chinese).

[13] FU G, WANG J Q, ZHANG M G, et al. An observational and numerical study of a sea fog event over the Yellow Sea on 11 April, 2004 [J]. Period Ocean Univ China, 2004, 34(05): 720-726 (in Chinese).

[14] GAO S H, LIN H, SHEN B, et al. A heavy sea fog event over the Yellow Sea in March 2005: Analysis and numerical modeling [J]. Adv Atmos Sci, 2007, 24 (1): 65-81.

[15] GAO S H, Qi Y L, ZHANG S B, et al. Initial conditions improvement of sea fog numerical modeling over the Yellow Sea by using cycling 3DVAR Part I: WRF numerical experiments [J]. Period Ocean Univ China, 2010, 40(10): 1-9 (in Chinese).

[16] ZHANG S P, REN Z P. The influence of the thermal effect of underlaying surface on the spring sea fog over the Yellow Sea: observations and numerical simulations [J]. Acta Meteorol Sinica, 2010, 68 (4): 439-449 (in Chinese).

[17] HEO K Y, HA K J. A Coupled Model Study on the Formation and Dissipation of Sea Fogs [J]. Mon Wea Rev, 2010, 138 (4): 1 186-1 205.

[18] KIM C K, YUM S S. A numerical study of sea-fog formation over cold sea surface using a one-dimensional turbulence model coupled with the weather research and forecasting model [J]. Bound-Layer Meteorol, 2012, 143 (3): 481-505.

[19] LI P Y, FU G, FU D, et al. The formation mechanism of a spring sea fog event over the Yellow Sea associated with a low-level jet [J]. Wea Forecast, 2012, 27: 1 538-1 553.

[20] ZHAO D C, LI Y, PAN X B, et al. Simulation of a sea fog event using a WRF-POM model [J]. Marine Forecast, 2014, 31(1): 77-85 (in Chinese).

[21] WANG B H. Sea Fog [M]. Beijing: China Ocean Press, 1983 (in Chinese).

[22] HUANG J, WANG B, ZHOU FX, et al. Turbulent heat exchange in a warm sea fog event on the coast of South China [J]. Chin J Atmos Sci, 2010, (04): 715-725 (in Chinese).

[23] HUANG H J, HUANG J, LIU C X, et al. Microphysical characteristics of the sea fog in Maoming area [J]. Acta Oceanol Sinica, 2009, (02): 17-23 (in Chinese).

[24] HUANG H J, HUANG J, MAO W K, et al. Characteristics of liquid water content of sea fog in Maoming area and its relationship with atmospheric horizontal visibility [J]. Acta Oceanol Sinica, 2010, (02): 40-53 (in Chinese).

[25] HUANG H J. Observational analysis of sea fog and its boundary layer structure on the coast of Southern China [D]. Ph.D. dissertation, Nanjing University, 2013, 129 pp. (in Chinese).

[26] HUANG H J, LIU H N, JIANG W M, et al. Characteristics of the Boundary Layer Structure of Sea Fog on the Coast of Southern China [J]. Adv Atmos Sci, 2011, 28 (6): 1 377-1 389.

[27] HUANG H J, LIU H N, HUANG J, et al. Atmospheric boundary layer structure and turbulence during sea fog on the southern China coast [J]. Mon Wea Rev, 2015, 143, 1 907-1 923.
[28] HUANG H J, HUANG J, LIU C X, et al. Prediction of sea fog of Guangdong coastland using the variable factors output by GRAPES model [J]. J Trop Meteorol, 2011, 17(2): 182-190.
[29] HUANG H J, HUANG J, LIU C X, et al. Improvement of regional prediction of sea fog on Guangdong coastland using the factor of temperature difference in the near-surface layer [J]. J Trop Meteorol, 2016, 22 (1): 66-73.
[30] HUANG J, HUANG H J, HUANG M H, et al. Decision tree forecasting models of sea fog for the coast of Guangdong province [J]. J Appl Meteorol Sci, 2011, 22 (1): 107-114 (in Chinese).
[31] YUAN J N, HUANG J. An observational analysis and 3-dimensional numerical simulation of a sea fog near Pearl River Mouth in boreal spring [J]. Acta Meteorol Sinica, 2011, 69(05): 847-859 (in Chinese).
[32] MLAWER E J, TAUBMAN S J, BROWN P D, et al. Radiative transfer for inhomogeneous atmosphere: RRTM, a validated correlated-k model for the longwave [J]. J Geophys Res, 1997, 102 (D14): 16 663-16 682.
[33] DUDHIA J. Numerical study of convection observed during the winter monsoon experiment using a mesoscale two-dimensional model [J]. J Atmos Sci, 1989, 46: 3 077-3 107.
[34] CHEN F, DUDHIA J. Coupling an advanced land-surface/ hydrology model with the Penn State/ NCAR MM5 modeling system. Part I: Model description and implementation [J]. Mon Wea Rev, 2001, 129: 569-585.
[35] ZHANG D L, ANTHES R A. A high-resolution model of the planetary boundary layer-sensitivity runs and comparisons with SESAME-79 data [J]. J Appl Meteorol, 1982, 21: 1 594-1 609.
[36] HONG S Y, NOH Y, DUDHIA J. A new vertical diffusion package with an explicit treatment of entrainment processes [J]. Mon Wea Rev, 2006, 134: 2 318-2 341.
[37] LIN Y L, FARLEY R D, ORVILLE H D. Bulk parameterization of the snow field in a cloud model [J]. J Climate Appl Meteorol, 1983, 22: 1 065-1 092.
[38] KAIN J S. The Kain-Fritsch convective parameterization: An update [J]. J Appl Meteorol, 2004, 43: 170-181.
[39] HUANG J, CHAN P. Progress of marine meteorological observation experiment at Maoming of South China [J]. J Trop Meteorol, 2011, 17: 418-429.
[40] BOLTON D. The computation of equivalent potential temperature [J]. Mon Wea Rev, 1980, 108: 1 046-1 053.
[41] LI Y A, CAO L, GAO S, et al. The current stage and development of MICAPS [J]. Meteorol Mon, 2010, 36 (7): 50-55 (in Chinese).
[42] FOKEN T, GÖCKEDE M, MAUDER M, et al. Post-field data quality control. Handbook of Micrometeorology: A Guide for Surface Flux Measurement and Analysis. Dordrecht: Kluwer Academic Publishers, 2004, 181-208.
[43] PLATNICK S and Coauthors, The MODIS cloud products: Algorithms and examples from Terra [J]. IEEE T Geosci Remote, 2003, 41: 459-473.
[44] DRAXLER R R, HESS G D. An overview of the HYSPLIT_4 modeling system of trajectories, dispersion, and deposition [J]. Aust Meteorol Mag, 1998, 47: 295-308.
[45] THIÉ BAUX J, ROGERS E, WANG W Q, et al. A new high-resolution blended real-time global sea surface temperature analysis [J]. Bull Amer Meteorol Soc, 2003, 84: 645-656.
[46] ROGERS D P, TELFORD J W. Metastable Stratus tops [J]. Quart J Roy Meteorol Soc, 1986, 112 (472): 481-500.

Citation: HUANG Hui-jun, ZHAN Guo-wei, LIU Chun-xia et al. A case study of numerical simulation of sea fog on the southern China coast [J]. J Trop Meteorol, 2016, 22(4): 497-507.